Available online at www.sciencedirect.com
ScienceDirect
Polymer 48 (2007) 2404–2414
polymer
www.elsevier.com/locate/polymer

# Fast isothermal calorimetry of modified polypropylene clay nanocomposites

V.V. Ray [a,b], A.K. Banthia [b], C. Schick [a,*]

[a] University of Rostock, Institute of Physics, 18051 Rostock, Germany
[b] Indian Institute of Technology, Kharagpur, India

Received 17 November 2006; received in revised form 18 February 2007; accepted 19 February 2007
Available online 28 February 2007

**Abstract**

Calorimetric experiments at cooling rates comparable to those during injection molding, as an example, are needed to study phase transitions under conditions relevant for processing. Ultra fast scanning calorimetry is a technique which provides a means to analyze the materials of interest under rapid cooling conditions and it is a promising technique by which the crystallization behavior of composite systems based on fast crystallizing polymers like isotactic polypropylene (iPP) can be studied. By combining conventional DSC and ultra fast chip calorimetry isothermal crystallization experiments were performed in the whole temperature range between glass transition and melting temperature of iPP. Because of the very small time constant of the calorimeter, isothermal crystallization processes with peak times down to 100 ms were investigated after cooling the sample from the melt at 2000 K/s. iPP grafted with maleic anhydride (PPgMA) − montmorillonite clay nanocomposites were studied. The influence of various clay loadings on the crystallization behavior of PPgMA at different temperatures was followed by ultra fast isothermal calorimetry. PPgMA clay nanocomposites showed a variation in crystallization peak times with different clay loadings at crystallization temperatures between 70 °C and 100 °C. No influence of clay loading was observed at lower crystallization temperatures. At these temperatures, where the mesophase is formed and homogeneous nucleation is expected, the contribution of the clay as a nucleating agent is negligible. For crystallization at about 80 °C, where the α-phase is formed, the nucleating effect of the clay is observed yielding complex crystallization kinetics. In the temperature range 75−85 °C in some nanocomposites a double peak during isothermal crystallization was observed corresponding to a fast and a slow crystallization processes occurring simultaneously. At higher temperatures, above 120 °C, the clay slightly retards the crystallization process.


*Keywords:* Polypropylene; Crystallization kinetics; Ultra fast scanning calorimetry

## 1. Introduction

Polypropylene (PP) is an important semi-crystalline thermoplastic material and is used in many different forms and applications through a range of manufacturing processes. Polypropylene offers a very attractive combination of physical and mechanical properties at a relatively low cost, which makes it a versatile material with continuously increasing applications. As such, polypropylene is one of the most studied polymers, its structure and properties are well documented, see e.g. the more than 6000 hits for ''polypropylene crystal*'' in SCOPUS™ [1]. But despite all these efforts important questions regarding crystallization are not completely answered. To mention only one: the influence of nanoparticles on crystallization in iPP is still controversially discussed, see e.g. Refs. [2–9].

The most common crystal modification, formed under normal processing conditions for commercial grades of isotactic polypropylene (iPP), is the monoclinic α form, first identified by Natta and Corradini [10]. A highly disordered mesomorphic phase can be obtained by quenching, see e.g. Ref. [11] and references therein. The mesomorphic phase has a lower melting point and is less stable. It transforms during heating into the more stable α form. According to literature for the mesomorphic form in quenched iPP melting and subsequent recrystallization into the α form occurs in the temperature range 40−80 °C [11–13]. The other two known crystalline

* Corresponding author. Tel.: +49 381 498 6880; fax: +49 381 498 6882.
*E-mail address:* christoph.schick@uni-rostock.de (C. Schick).

0032-3861/$ - see front matter © 2007 Elsevier Ltd. All rights reserved.
doi:10.1016/j.polymer.2007.02.055

forms of isotactic polypropylene are the β and the γ modifications. iPP's ability to crystallize in the β form was discovered by Keith et al. in the late 1950s [14], while the γ form was discovered by Addink and Beintema in 1961 [15]. It was found that these crystal forms can only be obtained by special modification of the crystallization conditions (e.g. by the use of specific nucleants or crystallization in the presence of shear and, in case of the γ modification, by the presence of small amounts of comonomers or sterio or regio defects, see e.g. [16] and references therein). For a review regarding the different polymorphs of iPP see Ref. [17].

In recent years, a lot of interest from both, academia and industry has been attracted to the study of polymer nanocomposites, in which a polymer matrix is reinforced with a dispersed phase with at least one dimension in the range of 1–100 nm. Recent efforts have focused upon polymer-layered silica nanocomposites and other polymer–clay composites due to their improved properties. Polymer-layered silicate nanocomposites (PLSN) are scientifically interesting because of the new nanoscale constraints of the filler to the polymer matrix and the ultrahigh specific interfacial area between the silicate and the matrix [18]. These materials have improved mechanical properties without the large loading required by traditional particulate fillers. This enhancement is already obtained with silicate loadings as low as 1–4 volume percentage [18]. Silicate type minerals like talc and mica are well known nucleating agents too [19]. So these nanosized silicate layers may act as nucleating agents in the crystallization of the polymer matrix.

Wu et al. [20] observed an unusual crystallization behavior in PA6/MMT nanocomposites, namely that increased cooling rate would result in higher crystallinity of PA6/MMT nanocomposite in sharp contrast to pure PA6 and other semicrystalline polymers and the γ form crystal was dominant in the rapidly cooled nanocomposite. Solomon [4] and Nowak [5] investigated the early stage of shear-induced crystallization in PP/MMT nanocomposites. For quiescent isothermal crystallization, the intercalated iPP nanocomposite displayed retarded crystallization kinetics compared to that of pure iPP. Such a retarding effect of the silicate layers on the crystal growth of polymer matrices has been reported in Refs. [6,7] too. In crystallization of extruded PA6/MMT nanocomposites, the overall crystallization rate decreases with increasing silicate layer content at the highest silicate layer contents or even over the full silicate layer content range. It was postulated that during the crystallization of the matrix polymer the silicate layers act as non-crystallizable barriers, especially at high concentration, disturbing crystal growth by forcing the growing lamellar stacks along a more tortuous growth path. Another possibility is that the silicate layers hinder polymer chain motion [6].

The isothermal crystallization kinetics of maleic anhydride grafted polypropylene (PPgMA) in hybrids with unmodified or organically modified montmorillonite (MMT), which have been prepared by melt intercalation in a mixer, has been investigated by Baekjin Kim et al. [7], and showed that the PPgMA/unmodified MMT hybrids formed macrophase-separated mixtures rather than intercalated nanocomposites, while PPgMA/organically modified layered silicate (OLS) hybrids formed exfoliated nanocomposites. The crystallization rate of PPgMA/unmodified silicate hybrids became faster with the MMT addition and the crystallization rate of the PPgMA/OLS hybrids was slowed down with the OLS addition [7].

Beside chemical structure and composition the properties of synthetic polymer products are determined equally well by the processing step. Therefore analytical techniques are needed which allow investigations under conditions similar to processing. Ultra fast scanning (chip) calorimetry belongs to this kind of techniques providing information on thermodynamic properties and structure changes in materials at high-speed thermal treatments on cooling and on heating [13,21–23], as well as on size dependent effects in thin polymer films and nanoparticles [24–27]. The actual thermodynamic state of a semi-crystalline polymer, as an example, can be investigated only at sufficiently high heating rates of the order $10^3$ K/s and even more. Such high cooling and heating rates are required to prevent crystallization or reorganization of the sample during the scan. Only then, as an example, it is possible to study exclusively the melting of the crystals originally present in the sample [28–31]. Such non-equilibrium states may be generated by rapid cooling during processing. Therefore, calorimetric experiments at cooling rates comparable to that during injection molding, as an example, are needed to study phase transitions under processing conditions. With common DSC apparatus, like the Perkin Elmer Instruments Pyris DSC, calorimetric measurements at constant cooling rates up to 8 K/s can be realized which is still too slow to mimic realistic cooling conditions at injection molding of thin walled products which may reach hundreds or even thousands of Kelvins per second [32].

In this work an attempt was made to utilize the benefits of ultra fast scanning calorimetry to study the influence of clay on the crystallization kinetics of maleic anhydride grafted polypropylene (PPgMA) layered silica nanocomposites at different temperatures. Combining fast scanning chip calorimetry and DSC allows studying isothermal crystallization in the whole temperature range between melting temperature and glass transition temperature. Crystallization was followed on time scales covering the range from 100 ms up to hours. The influence of the nano-filler on the crystallization kinetics was studied for the first time in the temperature range of homogeneous as well as heterogeneous nucleation of the fast crystallizing polymer directly. The study is thought to help to understand some of the contradicting results reported for similar systems recently [4,7] and to demonstrate the possibilities of chip based nanocalorimetric sensors, even if it does not provide definite answers.

## 2. Experimental

### 2.1. Materials

*Polymer matrix*: Polypropylene grafted maleic anhydride (PPgMA) with a mass fraction of 0.6% maleic anhydride (Aldrich Chemical Company, USA).

*Nano-filler*: Cloisite 20A (Southern Clay products, USA), a quaternary ammonium salt modified natural montmorillonite polymer additive.

*Nanocomposites*[1]: PPgMA + 2.5, 5, 7.5 and 10 wt% Cloisite 20A nanocomposites were prepared by melt blending [33]. The material was extruded (Haake Rheomex, TW 100, Twin screw extruder with intermeshing screws, 40 cm), at 185 °C and 50 $min^{-1}$. Nanocomposite films were made using a hydraulic press with two heated plates (Bucher plastics press KHL100) at 165 °C and applying a pressure of 120 bar. The whole preparation process was optimized by varying the process conditions to obtain nanocomposites with largely delaminated structures [33]. The TEM investigation (Fig. 1) of the nanocomposite revealed predominant absence of large, undisturbed clay particles and the material seemed to be well exfoliated in structures about 100–200 nm long, consisting of intercalated stacks comprising one to five silicate layers [33,34]. The same samples were also thoroughly investigated by dielectric spectroscopy [35] where from an interfacial relaxation process a well exfoliated distribution of the clay platelets was confirmed too.

The manufactured composite samples were obtained as such and were used for analysis without further processing other than cutting appropriate samples from the films.

## 2.2. Methods

### 2.2.1. Differential scanning calorimetry

A Pyris Diamond Differential Scanning Calorimeter (Perkin Elmer Inc., USA) equipped with an intracooler was utilized for non-isothermal as well as isothermal crystallization experiments. The calorimeter was calibrated by indium and zinc as usual [36], nitrogen was used as purge and sample mass was about 5 mg. Non-isothermal experiments were carried out by cooling the samples from 200 °C at cooling rate 10 K/min. Isothermal experiments were carried out by heating the samples to the molten state (pure PPgMA to 200 °C, the nanocomposites to 180 °C) and immediate cooling to different crystallization temperatures at a rate of 100 K/min. The isothermal crystallization experiments were limited to the temperature range between about 120 and 150 °C. At higher temperatures the exothermic peak was not well developed because of the small heat flow and at lower temperatures crystallization became too fast to be correctly resolved by the DSC. In order to extend the temperature range to lower temperatures the ultra fast chip calorimeter was used [37].

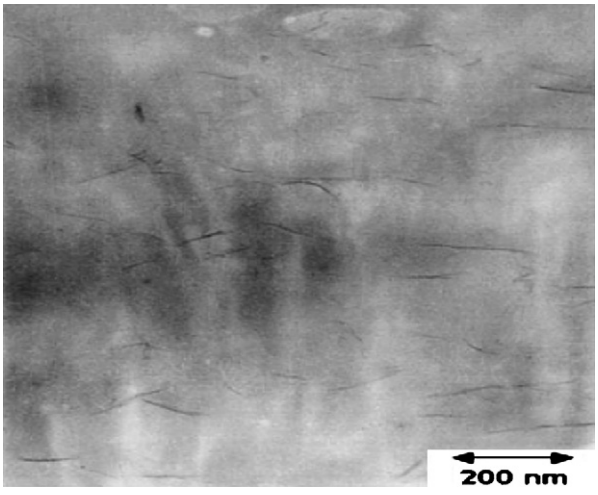


Fig. 1. TEM micrograph of PPgMA Cloisite 20A (5%) nanocomposite (adapted from Ref. [33]).

### 2.2.2. Ultra fast chip calorimeter

For ultra fast chip calorimetry (Fig. 2) a commercial thin film vacuum sensor, thermal conductivity gauge TCG 3880, Xensor Integrations, The Netherlands [38] was used. The thermal conductivity gauge TCG 3880 consists of a ca. 500 nm thick $Si_3N_x$ membrane with a semi-conductive film thermopile and a semi-conductive resistive film heater, ca. 50 μm × 100 μm, placed at the center of the membrane. The thermopile hot junctions are arranged around the heater at a distance of ca. 50 μm from the heater. The cold junctions are placed at the periphery of the cell ca. 1 mm from the center where the membrane is attached to the holder. Thus the cold junction temperature is the temperature of the holder and it is close

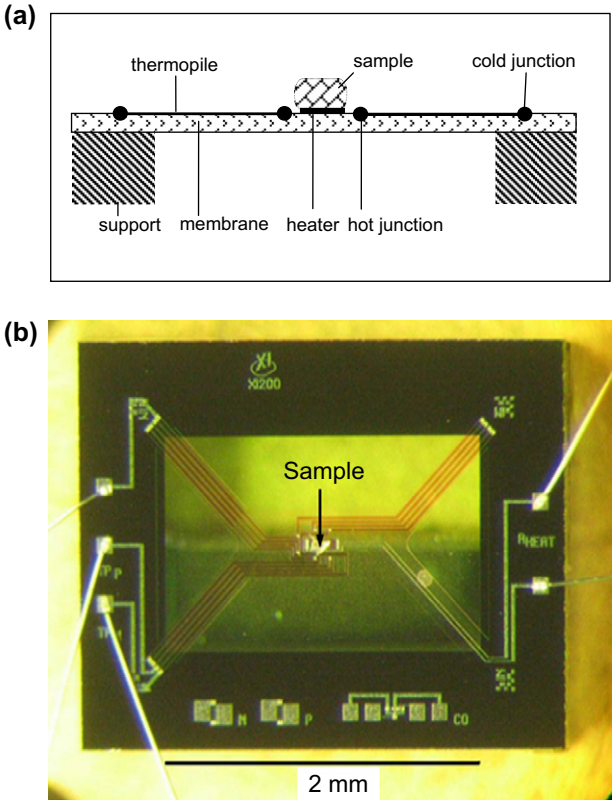


Fig. 2. Thin-film chip calorimeter based on the thermal conductivity gauge TCG 3880. Scheme (a) and micro-photograph of the frame and the membrane loaded with a sample (b) [28].

[1] The nanocomposites were provided by M. Bartholmai and B. Schartel from the Federal Institute for Materials Research and Testing (BAM), Berlin, Germany. For details see Ref. [33].

to the temperature of the thermostat. An additional copper constantan thermocouple was utilized for the measurement of the holder temperature, which was used as the reference temperature. To allow fast cooling the cell is operated in an ambient gas [21].

The benefit of the gauge TCG 3880 is that its central heated region is small enough to be considered as a point source of heat flow into the gas. This heat flow is proportional to the gas thermal conductivity and it can be estimated and calibrated. The temperature measured by the thermopile does not represent the temperature of the heater/sample interface [39]. The thermopile measures a temperature at the membrane around the heater at a distance of ca. 50 μm from the heater perimeter. This causes a time delay of the temperature measurement of a few milliseconds and has to be taken into account for calibration [39,40].

The sensor is placed in a temperature controlled vacuum shielded oven. The internal volume can be filled with gas at controlled pressure between 10 Pa and 100 kPa. In this study nitrogen at ambient pressure was used. The whole construction fits into a Dewar vessel with liquid nitrogen for cooling. Details of the calorimeter construction (Fig. 3) and of the electronics used are given in Refs. [21,27,37].

The heat capacity $C$ of the sample can be determined from the heat balance equation

$$(C + C_0)\frac{dT}{dt} = P_0 - \xi(T(t) - T_0) \quad (1)$$

where $C_0$ is the heat capacity of the heated part of the membrane and the surrounding gas (addenda heat capacity; $C_0 \approx$ 150 nJ/K at room temperature [21,28], determined from a measurement without sample), $dT/dt$ is heating or cooling rate, $P_0$ is the electrical power to the heater, $\xi$ is heat exchange coefficient, $T(t)$ is the temperature of the heated region of the membrane and $T_0$ is the temperature of the gas (of the holder). This equation is correct, provided the thermal thickness of the sample is small enough and the heat transfer from the membrane to the oven can be described by Newton's law. Details of heat capacity determination as well as temperature calibration are given elsewhere [21,28,39]. It should be mentioned that calibration of the TCG 3880 sensor is rather difficult because it was not designed as a calorimetric sensor [40]. Now special calorimetric sensors are available from Sensor Integration [38] and calibration is straightforward [41]. In order to avoid intensive discussion of calibration we describe basically uncalibrated scan data here.

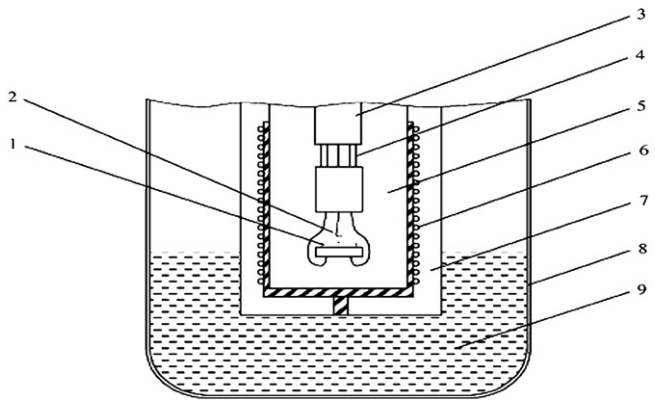


Fig. 3. The oven of the calorimeter: 1 – chip sensor, 2 – thermocouple to measure gas temperature, 3 – thin walled tube, 4 – connector, 5 – internal volume (pressure controlled), 6 – heater, 7 – external volume (vacuum), 8 – Dewar vessel, and 9 – liquid nitrogen [37].

For an isothermal crystallization experiment when $dT/dt \approx 0$ Eq. (1) simplifies in first approximation to

$$P_{cryst} - \xi(T(t) - T_0) = 0 \quad (2)$$

For all isothermal measurements crystallization temperature equals $T_0$. Therefore temperature calibration of the thermopile on the membrane is not important. Temperature calibration of the oven temperature $T_0$ was performed by an indium sample and results in an uncertainty of ±0.5 K. The temperature increase of the sample above the gas temperature $T(t) - T_0$ then provides a direct measure of the heat flow $P_{cryst}$ due to the exothermal crystallization event.

$$T(t) - T_0 = \frac{P_{cryst}}{\xi} \quad (3)$$

For such measurements crystallization temperature $T_c$ is assumed to equal $T_0$ even in some cases crystallization starts before $T_0$ is reached.

*2.2.2.1. Sample preparation.* The sample thickness must be small enough to avoid large temperature gradients perpendicular to the membrane. At a rate of $10^3$ K/s the temperature difference across a 10 μm thick sample is about 1 K ($\rho_s c_s = 2 \times 10^6$ J/Km$^3$ and $\lambda_s = 0.3$ W/Km) [39]. To avoid lateral temperature gradients on the periphery of the sample, outside the heater, the sample should be placed just on the heater. Therefore the sample was cut to very small pieces, ca. 150 ng, with a sharp knife. The smallest piece was selected and placed on the membrane. Then it was moved just on top of the heater. The movement to the right position was performed under a microscope by means of a thin copper wire, not to destroy the membrane. When the exact position was reached, the sample was melted by switching on the current to the heater. The sample was plate like after melting. The thermal contact between the heater and a thin sample is sufficiently good because of adhesive forces [21]. The cell with the sample was placed in the thermostat.

For such small samples homogeneity of the material becomes a serious issue. For the samples studied here no inhomogeneities were detected. Optical and TEM micrographs as well as repetition of measurements with different pieces from the same sample did not reveal inhomogeneities or differences in sample properties beyond experimental uncertainty for the 150 ng samples. Only the double peak, seen in some measurements as discussed below, was not highly reproducible.

*2.2.2.2. Measurements.* The calorimeter was placed in the gas volume of a nitrogen Dewar to attain low temperatures, i.e.

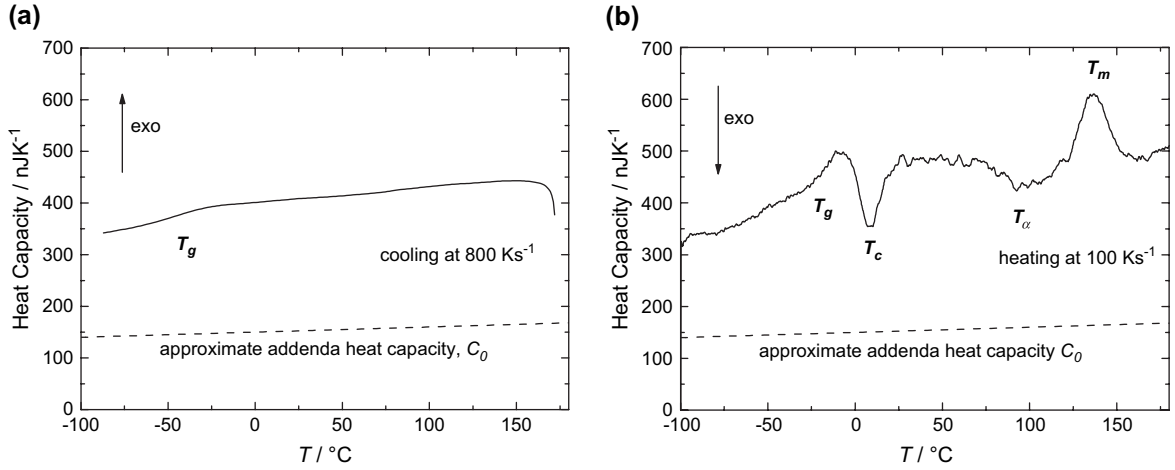


Fig. 4. Fast scanning of pure PPgMA. Raw data without extensive calibration neither for heat capacity nor for temperature. Here uncertainty for heat capacity is about ±20% and for temperature ±25 K (note, for the isothermal experiments discussed below it is about ±2 K, as described in Section 2). The approximate addenda heat capacity is indicated by the dashed lines. (a) Cooling at 800 K/s — crystallization is totally suppressed — only the glass transition ($T_g$) is seen. (b) Subsequent heating of the same sample at 100 K/s showing glass transition ($T_g$) followed by cold crystallization of the mesophase ($T_c$), recrystallization to the α-phase ($T_\alpha$) and final melting ($T_m$).

−100 °C in this study. The thermostat was set to the appropriate start temperature, which equals crystallization temperature as shown in Fig. 5 [37]. The inner chamber of the calorimeter was filled with nitrogen in order to avoid oxidative degradation of the sample at higher temperatures.

Non-isothermal experiments were carried out at different heating and cooling rates. Initially the sample was heated slightly above the melting temperature to determine the melting point at a heating and cooling rate of 100 K/s. Once the melting peak was observed, the cooling rate was increased up to 5000 K/s. From these measurements particular heating and cooling rates were selected to perform the further isothermal crystallization studies which were 100 K/s for heating and 2000 K/s for cooling. With such a high cooling rate, crystallization was completely suppressed in the cooling cycle; see also Ref. [13].

At rates above 400 K/s no crystallization on cooling was observed for all samples under investigation, an example at 800 K/s is shown in Fig. 4a. Consequently, isothermal crystallization experiments could be performed at any temperature between melting and glass transition temperatures by cooling the sample at 2000 K/s to the respective crystallization temperature. The subsequent heating scan at moderate heating rates shows the glass transition, cold crystallization towards the mesomorphic phase, recrystallization to the α-phase and melting of the α-phase, see Fig. 4b. At higher rates the cold crystallization and the recrystallization peaks are decreased and not well separated, see Ref. [23] for details.

Isothermal experiments were carried out at different temperatures by selecting each of these temperatures as the base temperature (temperature of the oven) starting from −5 °C to 100 °C, i.e. heating from the base temperature to slightly above the melting temperature and then fast cooling at 2000 K/s back to the base temperature. Isothermal crystallization was followed by the temperature increase of the membrane due to the exothermic crystallization process [37]. The

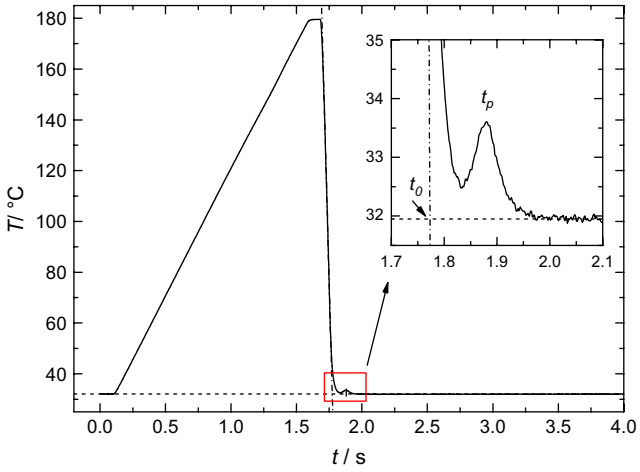


Fig. 5. Isothermal crystallization of pure PPgMA at 32 °C. The whole temperature time profile including melting and quenching at the crystallization temperature is shown. The inset presents the enlarged part just after reaching the crystallization temperature including the exothermic crystallization peak.

observed peak in the temperature time profile was used to determine a crystallization peak time, $t_{cp}$, and for a direct comparison of the shape of the crystallization peaks. It should be mentioned that in calorimetry always overall crystallization is followed and there is no easy way to separate nucleation and growth.

The crystallization peak time, $t_{cp}$, was determined in the following way. First a straight line parallel to the time axis and coinciding with the isothermal portion at the very end of the temperature profile was drawn, dashed line in Fig. 5. This line was used as the base temperature of the isothermal crystallization experiment and is given in all further graphs as the nominal isothermal crystallization temperature, $T_c$, even crystallization may already start at slightly higher temperature at the end of the cooling part. Next the linear section

of the cooling scan was linearly extrapolated to this horizontal line, dashed dotted line in Fig. 5. The origin of the time scale determined as the intersection of the two lines adds about 50–100 ms to the time scale compared to the time at which the temperature actually reaches the crystallization temperature, see inset in Fig. 7 and Fig. 9a. But the linear extrapolation assures a highly reproducible determination of the origin of the time scale, $t_0$, which is needed for a reliable determination of the crystallization peak time for different samples. The time of the maximum of the peak, $t_p$, was determined from the measured curve, inset of Fig. 5, and the difference $t_p - t_0$ was taken as the crystallization peak time, $t_{cp}$. The real crystallization peak time may be 50–100 ms shorter than the times reported below. But for the conclusions drawn from the measurements this offset is not important.

A more serious problem regarding determination of the absolute value of crystallization peak time than the definition of the origin of the time scale is that at many temperatures the crystallization starts before reaching the set crystallization temperature. This happens because at the very end of cooling the approach to the set temperature is exponential and depends slightly on sample properties; see also Ref. [23]. But following always the same procedure makes comparison of the data for the different samples possible.

For a direct comparison of the peak shapes at different nominal crystallization temperatures the temperature increase above the set crystallization temperature (horizontal line in Fig. 5) and the time starting at the origin, determined as described above, are used for further discussion. In Fig. 6 an example is given.

If curves from different samples (different sample masses) should be compared the temperature difference must be normalized. From the scan measurements we know the heat capacity (J/K) of each sample in the melt, see Fig. 4. The measured heat capacity is the sum of the sample and the addenda heat capacity. Addenda heat capacity of the sensor TCG 3880 is about 150 nJ/K [21,28]. Subtracting this value from the measured data yields the sample heat capacity (J/K) which equals specific heat capacity (J/gK) times sample mass. Dividing the measured heat capacity just after the melting peak by the known specific heat capacity for iPP at the same temperature, which is available from ATHAS data bank [42], gives a rough estimate for the sample mass, $m_s$, assuming constant specific heat capacities for all samples at that temperature. Because of the heat capacity uncertainty of about 20% the values were not corrected for the clay contribution (less than 5% in heat capacity). Another estimate for the sample mass is available from the dimension of the sample. From optical micrographs under different view angles the order of magnitude of sample volume can be obtained and compared with the mass from the heat capacity to identify faulty heat capacity data. Finally, the temperature increase $\Delta T$ is normalized by the sample mass estimate from heat capacity. An example for a normalized curve is shown in the inset of Fig. 6.

Fig. 7 shows different measurements at set crystallization temperature 35 °C to check reproducibility of the measurements.

For the measurements with the same sample peak position is highly reproducible, ±10 ms. The inset shows the comparison of the curves for different samples on two different sensors. The new sensor XEN 3940 is significantly faster compared to the gauge TCG 3880 and provides a more correct value of the peak time because the set temperature is reached already after 20 ms. The shift between both curves is about 20 ms, which is because of the larger time constant of the TCG 3880. The observed scatter of the data shown below is due to uncertainties of the measurement as well as possible differences in sample composition of the very small samples (≈150 ng). In summary an uncertainty of the peak time of about ±50 ms must be considered. But for the same sample scatter of the peak time is less than ±10 ms, which is the important figure for the data presented below.

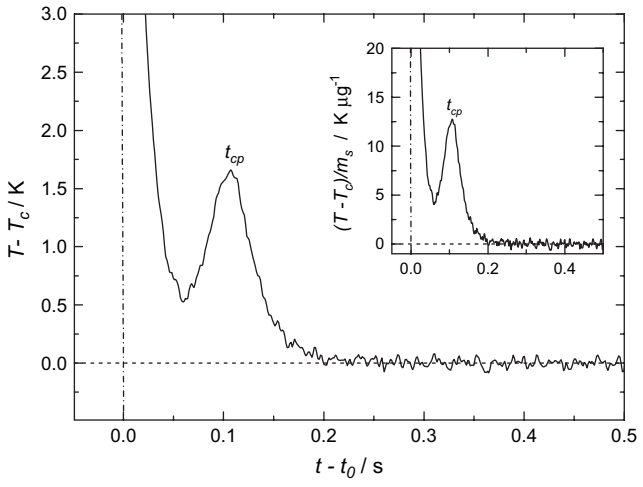


Fig. 6. Temperature difference vs. time difference. Pure PPgMA at crystallization temperature $T_c = 32$ °C. The inset shows the curve normalized by sample mass, $m_s \approx 130$ ng.

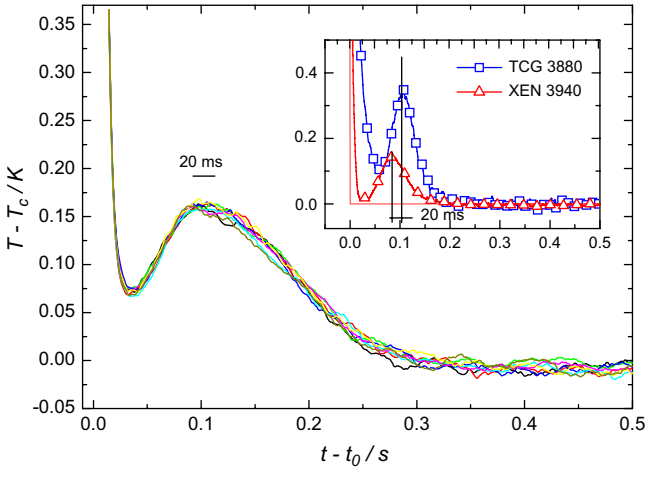


Fig. 7. Crystallization isotherms for PPgMA at 35 °C. The measurement was repeated eight times for the same sample. The inset shows the comparison of the same measurement with the sensors TCG 3880 and XEN 3940 [38] for different samples.

## 3. Results

### 3.1. Non-isothermal crystallization

The crystallization behavior of the nanocomposites was first followed by DSC. All samples were heated above the melting temperature followed by cooling at a rate of 10 K/min. At such rate non-isothermal crystallization occurs at about 118 °C (peak temperature) and is very much the same for all samples as shown in Fig. 8 and reported earlier [34]. For a direct comparison of the curves for the different samples the measured heat flow, $\Phi$, is normalized by polymer mass, $m_{\text{polymer}}$.

### 3.2. Isothermal crystallization

Because non-isothermal crystallization did not reveal significant differences in the crystallization behavior of the nanocomposites isothermal crystallization was followed by DSC and later on by fast scanning calorimetry. The samples were heated above the melting temperature at 200 °C and cooled at 100 K/min (ca. 2 K/s) in the DSC to the crystallization temperature. Then the exothermic heat flow, $\Phi$, due to crystallization is recorded as function of time.

At isothermal crystallization the nanoparticles influence crystallization kinetics a little (Fig. 9). With increasing filler content crystallization is slightly retarded. The effect is relatively small and in the logarithmic representation in Fig. 13, below, it is hard to see. At temperatures below 120 °C crystallization becomes too fast to resolve the maximum in the exothermic heat flow from the DSC curve.

As shown in Fig. 4 above no crystallization was observed on cooling at 800 K/s for the samples under investigation. Therefore isothermal crystallization experiments became possible in the whole range between melting and glass transition temperatures. The obtained crystallization peaks are shown for selected temperatures in Fig. 10. At −5 °C no crystallization occurs within 1 s because it is very close to the glass transition of the PPgMA. These curves show the approach towards the set temperature without any exothermic effect due to crystallization.

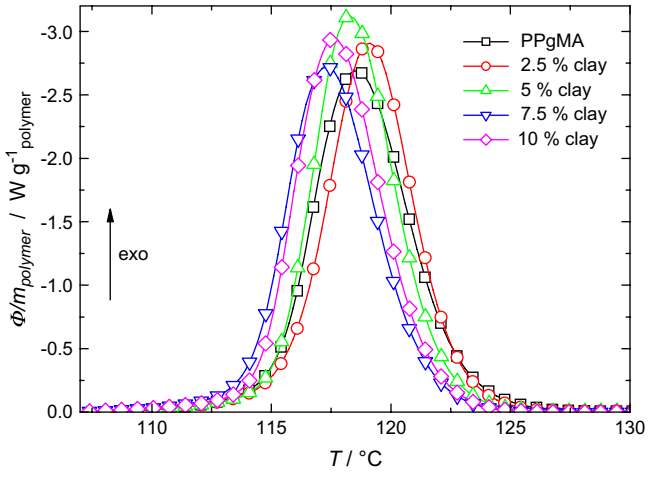


Fig. 8. Normalized excess heat flow, $\Phi/m_{\text{polymer}}$, during crystallization of pure PPgMA and the nanocomposites on cooling at 10 K/min. Pyris Diamond DSC, sample mass ca. 5 mg.

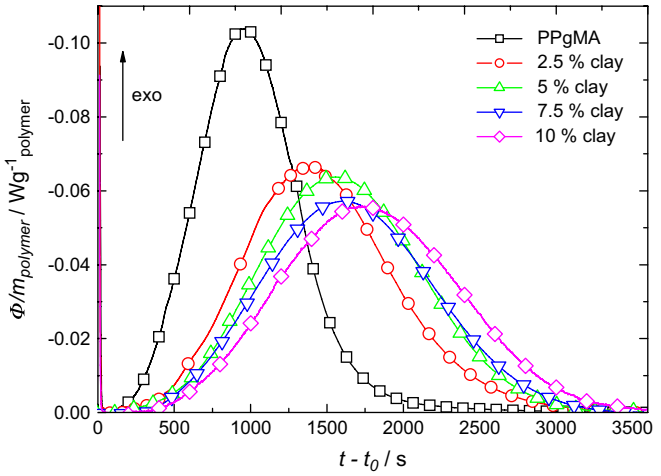


Fig. 9. Normalized heat flow, $\Phi/m_s$, during isothermal crystallization of pure PPgMA and the nanocomposites at crystallization temperature $T_c = 138$ °C. The origin of the time axis is determined as described above for the fast scanning experiments. Pyris Diamond DSC.

At $T_c = 35$ °C the exothermic crystallization peak is superimposed on the exponential decay of the temperature curves. For all clay loadings a similar behavior is observed. At $T_c = 75$ °C and $T_c = 80$ °C, depending on the filler content, differences in the crystallization kinetics are seen. In some curves even two maxima appear. The crystallization peak times, $t_{cp}$, for the different samples as a function of nominal crystallization temperature are shown in Figs. 11 and 13.

The observed behavior for PPgMA is typical for isotactic polypropylene (iPP) as reported in Refs. [43,44,23]. The two minima may be attributed to the formation of the mesophase at lower and the monoclinic α-phase at higher temperatures. But similar data were obtained for sPP [45] and poly(butylene terephthalate) [22] too, where no polymorphism under quiescent conditions is known. Therefore other explanations for the two minima should be considered too. Supaphol [45] discusses homogeneous and heterogeneous nucleation as the reason for the double bell shaped curves.

Approaching glass transition at low temperatures or melting at high temperatures slows down crystallization because of increasing viscosity or decreasing nucleation rate, respectively. Similar dependencies are observed for the different clay loadings.

Crystallization kinetics for all samples is very similar at temperatures below 60 °C. Around 80 °C the curves for the nanocomposites show a more complex behavior. In some cases a fast and a slow crystallization process is seen in one curve. The fast process becomes too fast at temperatures below 80 °C and can even not be resolved by the chip calorimeter. A curve showing both processes is shown in Fig. 12 together with a curve obtained at much lower temperature.

Crystallization peak times larger than 1 s, as observed for crystallization temperatures above 100 °C, cannot be resolved

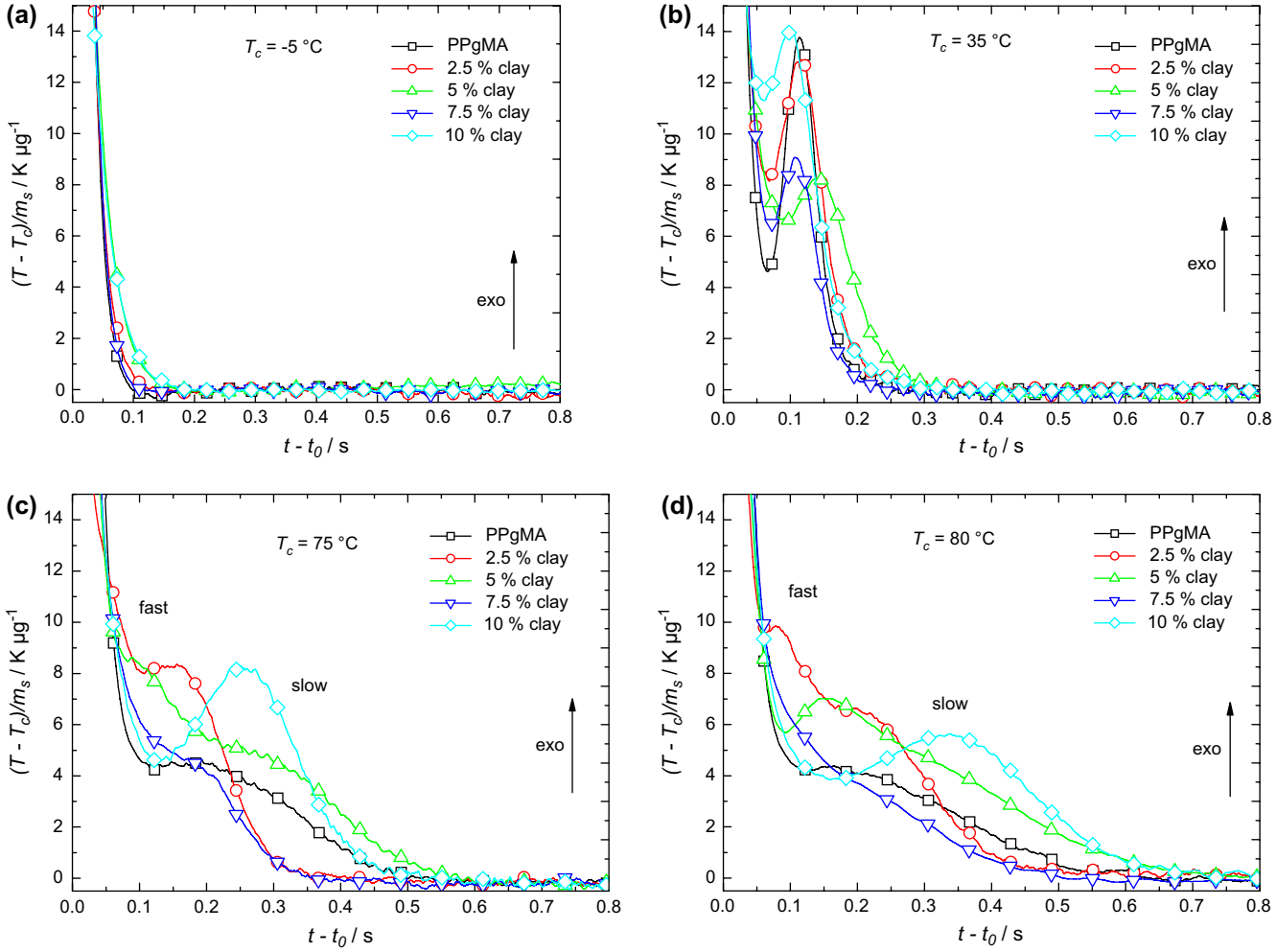


Fig. 10. Plots of normalized temperature difference vs. time difference for PPgMA and nanocomposites at $T_c = -5$ °C, 35 °C, 75 °C and 80 °C, respectively. Chip calorimeter.

by the chip calorimeter because the temperature increase becomes too small. In order to determine crystallization peak time at temperatures above 100 °C a Pyris Diamond Differential Scanning Calorimeter utilizing 4 orders of magnitude larger sample mass, ca. 5 mg, was used, see Fig. 9.

## 4. Discussion

The chip calorimeter curves at −5 °C, 35 °C, 75 °C and 80 °C for different clay loadings were compared, from which the variation of the shape of the curves with temperature can be seen. At −5 °C no peaks were observed indicating the absence of crystallization within the experimental time window of 1 s. The curves represent the exponential decay of the temperature towards the set temperature at the end of the scan. The curves allow an estimate of the time resolution of the device for the different samples. In any case after 150 ms isothermal conditions are realized.

At 35 °C, the temperature region where homogeneous nucleation is expected, the crystallization peaks are very sharp for all samples. The clay filler does not influence the behavior much.

The peaks are significantly broader at 75 °C and 80 °C and double peaks were observed for 2.5% and 5% clay loading. These two peaks are assigned to fast and slow crystallization kinetics occurring simultaneously in the nanocomposites. The fast process becomes too fast to be detected by the chip calorimeter below 80 °C. The reason for the occurrence of these two processes is not yet known. But they are present in the nanocomposites only. The differences between the curves seem to be real because it is much larger than the uncertainty of the peak time determination of ±50 ms.

At temperatures above 120 °C (Fig. 9) only a small retardation effect of the clay on crystallization is seen from isothermal DSC crystallization experiments. Crystallization peak time as function of crystallization temperature (Fig. 11) shows two shallow minima for all samples. The first between 10 °C and 30 °C and the second between 50 °C and 70 °C.

For the further discussion crystallization peak times from the chip calorimeter and the DSC measurements for all samples are combined in Fig. 13.

At temperatures below 60 °C the curves for all clay loadings are very similar. Between 70 °C and 100 °C the picture

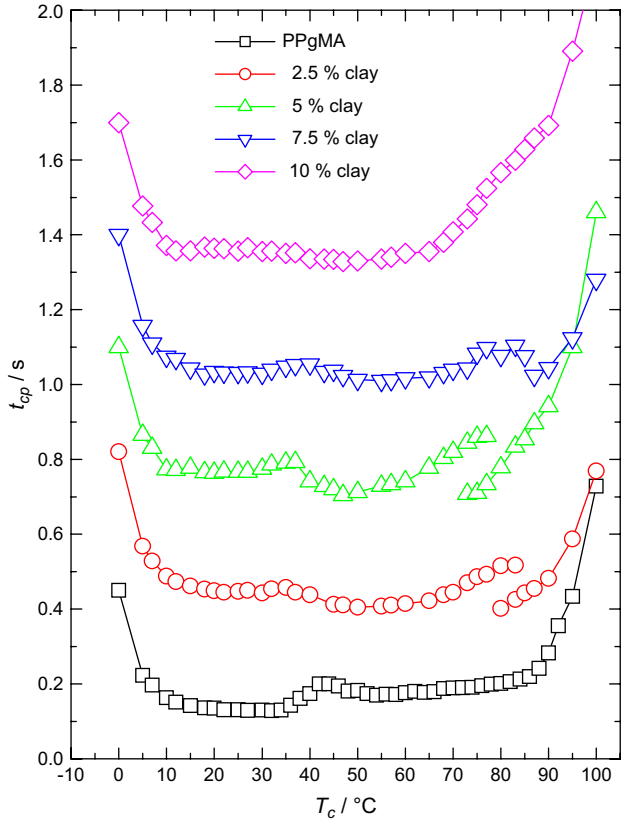


Fig. 11. Crystallization peak time vs. nominal crystallization temperature for PPgMA and the nanocomposites. The data from chip calorimeter are shifted successively by 0.3 s each. The PPgMA corresponds to the original scale.

is much more complex, see inset of Fig. 13. Two processes – a fast and a slow – can be observed. Around 80 °C a second mechanism sets in, which first coexists with the high temperature process and at lower temperatures it takes over the crystallization process in total. Only in this temperature range the nano-filler influences overall crystallization behavior

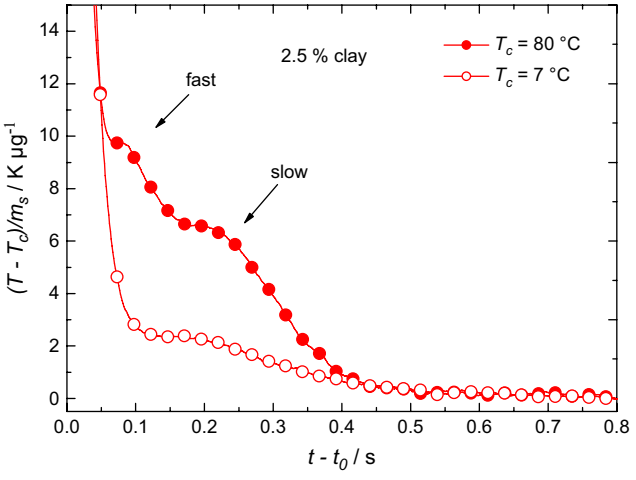


Fig. 12. Comparison of the double peak at 80 °C and single peak at 7 °C with similar crystallization peak times observed in the nanocomposite with 2.5% clay loading. Even the crystallization peak time is similar for the slow process the peaks are very different. Chip calorimeter.

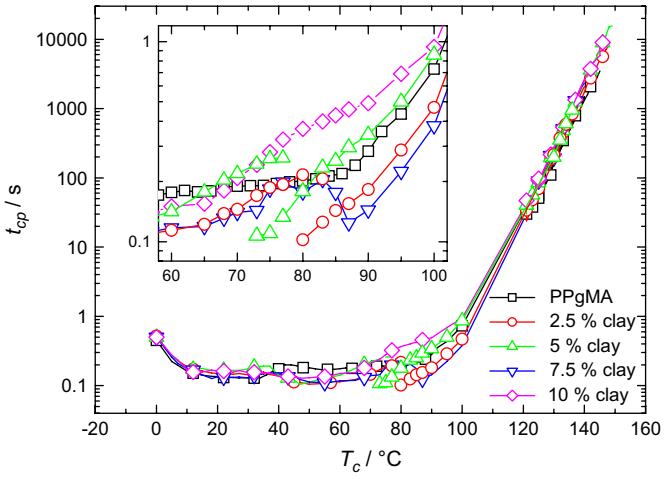


Fig. 13. Crystallization peak time on logarithmic scale vs. crystallization temperature for all samples. The inset shows the crystallization temperature range from 60 °C to 100 °C where the more complex behavior is observed. Measurements from chip calorimeter and DSC.

significantly. The nanocomposites exhibit a remarkable variation of the crystallization peak time from that of the pure PPgMA. The samples with 2.5% and 5% clay loadings showed a faster crystallization compared with the pure PPgMA and an interesting double peak effect, a fast crystallizing narrow peak and a slow crystallizing broad peak. In the case of 2.5% clay loading, this effect was observed in the temperature range of 70–85 °C and a well defined double peak was observed at 80 °C and for the 5% clay loading this was between 70 and 80 °C and the well defined double peak at 75 °C. The 7.5% clay loading also shows a more or less similar behavior in the temperature range of 90 °C. Even though the double peak was not observed, a fast crystallizing narrow peak was observed rather than the expected broad peak in this temperature range. The 10% clay loading shows a totally different behavior compared to the other three. Above 70 °C the sample crystallizes slower than the pure PPgMA.

The observed variation of the overall crystallization kinetics with temperature for the PPgMA and with the addition of clay may be described by different models. Next we try to explain the observations using terms like heterogeneous and homogeneous nucleation as well as retardation of crystal growth by the clay platelets following Supaphol's arguments [45]. Arguments are partly very weak and other explanations are possible too. Again, discussion is divided according the three temperature regions introduced above.

Below 60 °C, more evident below 40 °C, overall crystallization is independent on clay addition and very sharp crystallization peaks are observed at 35 °C. In this temperature region, where the mesophase is formed, a large number of small crystals, called nodules, are formed as shown e.g. by Zia and Androsch [11]. This is possible because of a large number of nuclei formed by homogeneous nucleation [45,46]. The crystals are growing simultaneously and yield a strong exothermic crystallization effect until space filling is achieved after relatively short time. Because crystallization

is limited in time a sharp peak as seen in Fig. 9b occurs. The large number of homogeneous nuclei results in a large number of small mesomorphic crystals. A more detailed Avrami analysis of the crystallization kinetics of unmodified iPP [23] also shows that the peaks at low temperatures can be best fitted assuming homogeneous nucleation ($n = 4$). The dominance of homogeneous nucleation is further supported by the nearly clay loading independent crystallization peak times in this temperature range. Addition of heterogeneous nuclei (clay particles) does not significantly alter the total number of nuclei because of the high homogeneous nucleation rate at those temperatures. The growth of the small nodules, on the other hand, cannot be retarded by the presence of the clay platelets because enough space is available between the clay platelets.

The situation is opposite at temperatures above 100 °C. Here the clay may act as nucleating agent but the increased number of nuclei may not be seen in overall crystallization because the growth of the relative large lamellar crystals could be hindered by the presence of the clay platelets, which have to be excluded from the growing lamellae. Such a mechanism seems to explain the observed retardation of the overall crystallization rate in the DSC measurements at high temperatures.

In the temperature range between 70 °C and 100 °C probability for homogeneous and heterogeneous nucleation by the clay may be similar. Nucleating activity of the clay platelets is known from several studies, e.g. Refs. [2,3,7–9,19]. At such temperatures, when overall crystallization rate in the unfilled sample is determined by the nucleation process, the addition of clay may alter crystallization rate. The fast process could be related to the crystallization in parts of the sample influenced by the nanoparticles (near the surface) and the slow process may occur in the bulk PPgMA [47]. From Fig. 13 no direct assignment can be made because the curve for the PPgMA lies somewhere in between the curves for the nanocomposites. No clear trend with nano-filler content is observed making an explanation very difficult. Another reason for the observed behavior could be the formation of two different crystal modifications in parallel. Obviously the interpretation is highly speculative and other experiments, characterizing the structure formed, are needed to allow a more serious discussion. But there is an experimental difficulty regarding the samples to be investigated. They have to be crystallized in this particular temperature range. It needs fast and controlled cooling, not easy to achieve for bulk samples. Experiments on a few micrometer thick films, as used for the nanoclaorimeter scans, are therefore needed.

## 5. Conclusions

Fast scanning calorimetry is a promising technique to analyze the crystallization behavior of fast crystallizing polymers like iPP and composite systems. Heating and cooling rates up to several thousand Kelvin per second, which are almost impossible with other calorimetric techniques, allow for a more detailed study of the crystallization kinetics. For the PPgMA – montmorillonite clay nanocomposites, a variation in isothermal crystallization peak times was observed with different clay loadings at crystallization temperatures between 70 °C and 100 °C. The increase in crystallization rate observed for 2.5% and 5% clay loadings may be due to the nucleating effect of the clay. A reduced crystallization rate with 10% clay loading reveals that the excess clay particles may act as hindrance for the polymer chains to crystallize, leading to a retardation effect. An interesting double peak effect was observed for the 2.5% and 5% clay loading around 80 °C, which may be due to the fact that both homogeneous and heterogeneous nucleation contributes to the crystallization process and this leads to a faster and a slower crystallization process taking place simultaneously in this particular temperature range.

These measurements may be useful in studies devoted to material processing, and can also be extended to blend systems based on fast crystallizing polymers. The crystallization behavior at various temperatures including the temperature range relevant for polymer processing can be studied.

## Acknowledgements

The authors acknowledge M. Bartholmai and B. Schartel, BAM, Berlin, Germany, for providing the nanocomposite samples and A.A. Minakov, J. Heeg and S. Adamovsky, Rostock, for helpful discussions and technical support. V.V. Ray acknowledges financial support from University of Rostock and Amrita Vishwa Vidyapeetham, India for sponsoring the Master of Technology program.

## References

[1] http://www.scopus.com/.
[2] Lincoln DM, Vaia RA, Wang Z-G, Hsiao BS. Secondary structure and elevated temperature crystallite morphology of nylon-6/layered silicate nanocomposites. Polymer 2001;42(4):1621–31.
[3] Maiti P, Nam PH, Okamoto M, Hasegawa N, Usuki A. Influence of crystallization on intercalation, morphology, and mechanical properties of polypropylene/clay nanocomposites. Macromolecules 2002;35(6):2042–9.
[4] Somwangthanaroj A, Lee EC, Solomon MJ. Early stage quiescent and flow-induced crystallization of intercalated polypropylene nanocomposites by time-resolved light scattering. Macromolecules 2003;36(7):2333–42.
[5] Nowacki R, Monasse B, Piorkowska E, Galeski A, Haudin JM. Spherulite nucleation in isotactic polypropylene based nanocomposites with montmorillonite under shear. Polymer 2004;45(14):4877–92.
[6] Fornes TD, Paul DR. Crystallization behavior of nylon 6 nanocomposites. Polymer 2003;44(14):3945–61.
[7] Baekjin Kim, Seung-Heon Lee, Daewon Lee, Bongwoo Ha, Joohyeon Park, Kookheon Char. Crystallization kinetics of maleated polypropylene/clay hybrids. Ind Eng Chem Res 2004;43(19):6082–9.
[8] Yuan Q, Awate S, Misra RDK. Nonisothermal crystallization behavior of polypropylene–clay nanocomposites. Europ Polym J 2006;42:1994–2003.
[9] Wang K, Liang S, Deng J, Yang H, Zhang Q, Fu Q, et al. The role of clay network on macromolecular chain mobility and relaxation in isotactic polypropylene/organoclay nanocomposites. Polymer 2006;47:7131–44.
[10] Natta G, Corradini P. Structure and properties of isotactic polypropylene. Nuovo Cimento Suppl 1960;15(1):40–51.
[11] Zia Q, Androsch R, Radusch H-J, Piccarolo S. Morphology, reorganization and stability of mesomorphic nanocrystals in isotactic polypropylene. Polymer 2006;47(24):8163–72.
[12] Wang Z-G, Hsiao BS, Srinivas S, Brown GM, Tsou AH, Cheng SZD, et al. Phase transformation in quenched mesomorphic isotactic polypropylene. Polymer 2001;42(18):7561–6.

[13] De Santis F, Adamovsky S, Titomanlio GM, Schick C. Scanning nanocalorimetry at high cooling rate of isotactic polypropylene. Macromolecules 2006;39(7):2562–7.
[14] Padden Jr FJ, Keith HD. Crystallization in thin films of isotactic polypropylene. J Appl Phys 1966;37(11):4013.
[15] Addink EJ, Beintema J. Polymorphism of crystalline polypropylene. Polymer 1961;2(2):185–93.
[16] Alamo RG, Kim Man-Ho, Galante MJ, Isasi JR, Mandelkern L. Structural and kinetic factors governing the formation of the γ polymorph of isotactic polypropylene. Macromolecules 1999;32:4050–64.
[17] Lotz B, Wittmann JC, Lovinger AJ. Structure and morphology of poly(propylenes): a molecular analysis. Polymer 1996;37:4979–92.
[18] Homminga D, Goderis B, Dolbnya I, Reynaers R. Crystallization behavior of polymer/montmorillonite nanocomposites. Part I. Intercalated poly(ethylene oxide)/montmorillonite nanocomposites. Polymer 2005; 46(25):11359–65.
[19] Wunderlich B. Macromolecular physics, vol. 2. New York: Academic Press; 1976. p. 35–52.
[20] Wu QJ, Liu XH, Berglund LA. An unusual crystallization behavior in polyamide 6/montmorillonite nanocomposites. Macromol Rapid Commun 2001;22(17):1438–40.
[21] Adamovsky S, Minakov AA, Schick C. Scanning microcalorimetry at high cooling rate. Thermochim Acta 2003;403(1):55–63.
[22] Pyda M, Nowak-Pyda E, Heeg J, Huth H, Minakov AA, Di Lorenzo ML, et al. Melting and crystallization of poly(butylene terephthalate) by temperature-modulated and superfast calorimetry. J Polym Sci B Polym Phys 2006;44(9):1364–77.
[23] De Santis F, Adamovsky S, Titomanlio G, Schick C. Isothermal nanocalorimetry of isotactic polypropylene. Macromolecules, submitted for publication.
[24] Allen LH, Ramanath G, Lai SL, Ma Z, Lee S, Allman DDJ, et al. 1,000,000-Degrees-C/S thin-film electrical heater – in-situ resistivity measurements of Al and Ti/Si thin-films during ultra-rapid thermal annealing. Appl Phys Lett 1994;64(4):417–9.
[25] Efremov MY, Olson EA, Zhang M, Zhang Z, Allen LH. Probing glass transition of ultrathin polymer films at a time scale of seconds using fast differential scanning calorimetry. Macromolecules 2004;37(12): 4607–716.
[26] Lupascu V, Huth H, Schick C, Wübbenhorst M. Specific heat and dielectric relaxations in ultra-thin PS layers. Thermochim Acta 2005;432(2): 222–8.
[27] Huth H, Minakov AA, Schick C. Differential AC-chip calorimeter for glass transition measurements in ultrathin films. J Polym Sci Part B Polym Phys 2006;44(20):2996–3005.
[28] Minakov AA, Mordvintsev DA, Schick C. Melting and reorganization of poly(ethylene terephthalate) on fast heating (1,000 K/s). Polymer 2004;45(11):3755–63.
[29] Minakov AA, Mordvintsev DA, Schick C. Isothermal reorganization of poly(ethylene terephthalate) revealed by fast calorimetry (1000 K $s^{-1}$; 5 ms). Faraday Discuss 2005;128:261–70.
[30] Tol RT, Minakov AA, Adamovsky SA, Mathot VBF, Schick C. Metastability of polymer crystallites formed at low temperature studied by Ultra fast calorimetry: polyamide 6 confined in sub-micrometer droplets vs bulk PA6. Polymer 2006;47(6):2172–8.
[31] Minakov AA, Mordvintsev DA, Tol R, Schick C. Melting and reorganization of the crystalline fraction and relaxation of the rigid amorphous fraction of isotactic polystyrene on fast heating (30,000 K/min). Thermochim Acta 2006;442(1–2):25–30.
[32] Brucato V, Crippa FG, Piccarolo S, Titomanilo G. Crystallization of polymer melts under fast cooling. 1. Nucleated polyamide-6. Polym Eng Sci 1991;31(19):1411–6.
[33] Bartholmai M, Schartel B. Layered silicate polymer nanocomposites: new approach or illusion for fire retardancy? Investigations of the potentials and the tasks using a model system. Polym Adv Technol 2004; 15(7):355–64.
[34] Tidjani A, Wald O, Pohl M-M, Hentschel MP, Schartel B. Polypropylene-*graft*-maleic anhydride-nanocomposites: I – characterization and thermal stability of nanocomposites produced under nitrogen and in air. Polym Degrad Stab 2003;82:133–40.
[35] Böhning M, Goering H, Fritz A, Brzezinka KW, Turky G, Schönhals A, et al. Dielectric study of molecular mobility in poly(propylene-*graft*-maleic anhydride)/clay nanocomposites. Macromolecules 2005;38: 2764–74.
[36] Sarge SM, Hemminger W, Gmelin E, Höhne GWH, Cammenga HK, Eysel W. Metrologically based procedures for the temperature, heat and heat flow rate calibration of DSC. J Therm Anal 1997;49(2):1125–34.
[37] Adamovsky S, Schick C. Ultra-fast isothermal calorimetry using thin film sensors. Thermochim Acta 2004;415(1–2):1–7.
[38] van Herwaarden AW. Overview of calorimeter chips for various applications. Thermochim Acta 2005;432(2):192–201, http://www.xensor.nl/.
[39] Minakov AA, Adamovsky SA, Schick C. Non adiabatic thin-film (chip) nanocalorimetry. Thermochim Acta 2005;432(2):177–85.
[40] Minakov AA, Morikawa J, Hashimoto T, Huth H, Schick C. Temperature distribution in a thin-film chip utilized for advanced nanocalorimetry. Meas Sci Technol 2006;17(1):199–207.
[41] Minakov AA, van Herwaarden AW, Wien W, Wurm A, Schick C. Advanced nonadiabatic ultrafast nanocalorimetry and superheating phenomenon in linear polymers. Thermochim Acta, submitted for publication.
[42] Wunderlich B. The ATHAS database on heat-capacities of polymers. Pure Appl Chem 1995;67(6):1019–26, http://athas.prz.rzeszow.pl.
[43] Schick C. General discussion. Faraday Discuss 2005;128:321–39.
[44] Silvestre C, Cimmino S, Duraccio D, Schick C. Isothermal crystallization of isotactic polypropylene by superfast calorimetry. Macromol Rapid Commun, in press.
[45] Supaphol P, Spruiell JE. Isothermal melt- and cold-crystallization kinetics and subsequent melting behavior in syndiotactic polypropylene: a differential scanning calorimetry study. Polymer 2001;42:699–712.
[46] Konishi T, Nishida K, Kanaya T. Crystallization of isotactic polypropylene from prequenched mesomorphic phase. Macromolecules 2006;39(23): 8035–40.
[47] Jean-Hong Chen, Bo-Xian Yao, Wen-Bin Su, Yao-Bin Yang. Isothermal crystallization behavior of isotactic polypropylene blended with small loading of polyhedral oligomeric silsesquioxane. Polymer 2007;48: 1756–69.